RESEARCH ARTICLE

Rehabilitation of SDOF systems under air blast loading with a modified negative stiffness amplifying damper

K. K. Kiran[1] · Ehsan Noroozinejad Farsangi[2] · Vahidreza Gharehbaghi[3] · Aleksandra Bogdanovic[4]

Abstract
Modified negative stiffness amplifying damper (MNSAD) is a novel vibration control device expected to consist of a negative stiffness spring with flexible cladding material. In this system, a dashpot is used in conjunction with the negative stiffness spring, and the damping magnification effect is greatly enhanced by amplifying the stoke of the dashpot. The negative stiffness property is preserved, and the MNSAD takes into account significant damping magnification effects. In this study, displacement and acceleration responses of SDOF systems under air blast load equipped with an MNSAD are investigated, which takes stochastic responses into account. Next, the optimum designed parameters yield three key parameters: stiffness ratio, damping ratio, and negative stiffness ratio. Following that, the SDOF system's responses to air blast load are calculated. It was observed that a significant damping effect is achieved by adding small damping (i.e., 2.8%) to the SDOF system with the proposed MNSAD. It was also discovered that replacing NSAD with MNSAD increases the long period structure's energy dissipation capacity from 16 to 28%.

Keywords SDOF · Air blast load · Negative stiffness amplifier damper · Modified negative stiffness amplifier damper · Stochastic response · Energy ratio · Resilience

1 Introduction

Detection of explosives in densely populated areas prevents injuries and saves many lives. Many people nowadays are afraid of explosives [1]. Countless people are killed as a result of blast load in the majority of the world, particularly in land mine zones and along country borders. In 2015, for example, approximately 713 people were killed due to explosions in land mine zones. Furthermore, in a more recent incident in Afghanistan, nearly 1000 people were killed as a result of improvised explosive devices [2–5]. As a result of rising terrorist activity, the safety and adaptability of infrastructure, particularly critical buildings, have become top global priorities [6–9]. Furthermore, hospitals, laboratories, technology centers, and computer facilities contain numerous non-structural components that are more expensive than the structure itself; as a result, these components must be protected against high impulse dynamic loads such as wind, blast, and earthquake load [10].

The axial and transverse directions of the blast load acting on the equivalent single degree of freedom (SDOF) system are studied using both experimental and analytical methods [11]. Many textbooks, manuals, and reports have used examples, charts, and failure mechanisms to describe the performance of SDOF systems subjected to non-linear blast load [12–15]. To that end, the surface blast load operating on the SDOF system's front face, rear face, and roof is computed and then regulated using a load cladding structural system [16]. SDOF systems with blast load performance, in particular, require fewer input parameters for calculation. As a result, many researchers have conducted research on the SDOF system when subjected to impact loads [17–20]. Similarly, the SDOF system of a blast-loaded plate can be experimentally and analytically analyzed, taking into account the bending behaviour of the plate [21–24].

✉ Ehsan Noroozinejad Farsangi
noroozinejad@kgut.ac.ir

1 SJB Institute of Technology, Bangalore, Karnataka, India

2 Faculty of Civil and Surveying Engineering, Graduate University of Advanced Technology, Kerman, Iran

3 School of Civil Engineering and Surveying, University of Southern Queensland, Springfield, QLD, Australia

4 Institute of Earthquake Engineering and Engineering Seismology, IZIIS, University "Ss. Cyril and Methodius", Skopje, Republic of North Macedonia

The air blast wave parameters have been predicted experimentally, analytically, and numerically [25–35]. For example, for different standoff distances acting on a masonry heritage building, air-blast pressure with and without ground shock generated by a spherical shaped TNT explosive is investigated experimentally and numerically [36]. The performance of an air-blasted polyurea-coated metal plate is investigated experimentally and analytically [37]. Others investigated the dynamic performance of welded aluminum plates subjected to an air blast load using experiments and numerical simulations [38]. Several researchers used experimental data and numerical simulations to investigate steel tubes subjected to an air blast load [39–41]. Others have also investigated the fluid–structure interactions associated with air blast loads [6].

Molyneaux pioneered vibration control of a system using a negative stiffness damper (NSD) in 1957 [42].

Nagarajaiah et al. [43], Sarlis et al. [44] provide useful details about the principle of the negative stiffness damper exposed to seismic load in this area. As an example, the bilinear SDOF elastic system of NSD placed on the first storey of the structure evaluates the performance of the MDOF system exposed to seismic load [45]. Linear Quadratic Regulator (LQR) algorithm mechanisms, on the other hand, rely on the principle of the force–displacement relationship of negative stiffness to control seismic responses [46]. For more information on the applications of the negative stiffness damper on the vibration control of vehicle suspensions and mechanical equipment, see references [47–49]. After a while, negative stiffness dampers are used to reduce the response of seismic structures [50]. In this context, [48, 50–58] investigates the improvement of seismic isolated structures and bridges using various semi-active damper combinations of the NSD. It should be noted that adaptive negative stiffness devices (NSDs) use pre-compressed springs [59–61].

The purpose of this study is to fill in the gap left by the literature review as follows:

(i) Developing the SDOF system's Modified Negative Stiffness Amplifying Damper (MNSAD) under air blast load.
(ii) Optimizing dynamic properties of the MNSAD.

Accordingly, this paper employs MATLAB software to perform numerical simulations of the SDOF system before investigating the effects of combining the negative stiffness device with cladding material. Many researchers have conducted studies on the seismic effects of the SDOF system based on the authors' knowledge. However, an attempt is made to investigate the responses of the SDOF system when subjected to an air blast load, with the responses controlled using MNSAD. Finally, the MNSAD and NSAD efficiency are compared under stochastic excitations and air blast load.

The background and origins of the research are discussed in the following section. Following that, the performance of the proposed method is evaluated, and the results are contrasted and discussed. Finally, there are conclusions and key points derived from this research.

2 Dynamic equations of MNSAD

First, some background information is provided to support the proposed strategy. Figure 1a depicts dashpot, positive and negative stiffness springs with an NSAD. As shown, the negative stiffness spring and dashpot are connected in parallel, whereas the previous configuration is connected in series with the positive stiffness spring. In addition, the positive spring in the NSAD has been replaced, and a new cladding material has been installed, resulting in the Modified negative stiffness amplifying damper (MNSAD), as illustrated in Fig. 1b. If only negative stiffness and series connections are made with positive stiffness springs while ignoring dashpot and cladding material of the NSAD and MNSAD as shown in Fig. 1c, static equilibrium stiffness KTE is demonstrated as follows [62]:

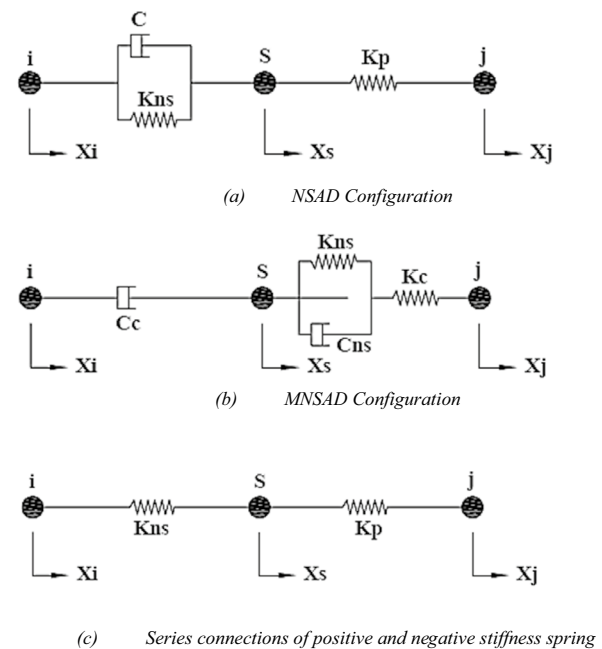$$K_{TE} = \frac{K_p K_{ns}}{K_p + K_{ns}} \tag{1}$$

(a)   NSAD Configuration

(b)   MNSAD Configuration

(c)   Series connections of positive and negative stiffness spring

Fig. 1 Relationship between positive stiffness spring, negative stiffness spring, and dashpot connection

where K_p and K_{ns} are the stiffness of the positive stiffness spring and negative stiffness spring, respectively. Static equivalent stiffness of the MNSAD is represented below:

$$K_{MTE} = \frac{K_C K_{ns}}{K_C + K_{ns}} \tag{2}$$

where K_{MTE} and K_c stand for the Static equivalent stiffness of the MNSAD and stiffness of the cladding material.

2.1 MNSAD physical realisation

Figure 2 shows the physical manifestations of the MNSAD. In this context, the researchers' previous results for NSAD [60, 63–65] are used to reduce seismic force response by replacing the viscous damper with cladding material. A viscous damper is a passive control device, whereas the cladding material is a semiactive control device. A pre-compressed spring, a pivot plate, a gap spring, and a self-contained system are all components of an NSAD. Many applications of the NSAD in real-world civil engineering structures are focused on the seismic effect of the structures. Nonetheless, in the current work, the inertia effect of the dynamic effect of the NSAD is ignored; this issue is considered within the analysis of the vibrations control of the structures.

Vicous dampers are installed in the NSD by replacing two gap springs [66]. The C_D shows the dashpot in Fig. 2, and the cladding material and NSD are connected in parallel. An ideal MNSAD configuration includes a dashpot with the negative stiffness spring and prior assembly connected in series and the positive stiffness spring and prior assembly connected in parallel. In this figure, K_p depicts the positive stiffness spring, and the NSAD cladding material is attached to the adjacent storey structure via a flexible supporting shelf connection.

2.2 MNSAD and transfer function of the equation of motion's SDOF systems

Figure 3 shows the simplified SDOF system in a one storey and one bay frame. In which m_1 shows the structural mass, k_1 is lateral stiffness, and c_1 is damping.

The dynamic equations of the SDOF system with blast load in terms of pressure versus time, ground accelerations $\ddot{x}_g$ is given as

$$\begin{cases} m_1\ddot{x}_1 + c_1\dot{x}_1 + k_1 x_1 + k_p(x_1 - x_2) = -m_1\ddot{x}_g - P(t) \\ C_c\dot{x}_2 + k_{ns}x_2 + C\dot{x}_1 = k_2(x_1 - x_2) \end{cases} \tag{3}$$

where C_2 is damping coefficient of the MNSAD, k_p shows the positive stiffness, k_c is the cladding material stiffness, k_2 is the positive stiffness of NSAD, x_1 stands for the relative displacement of the primary structure and deformations of
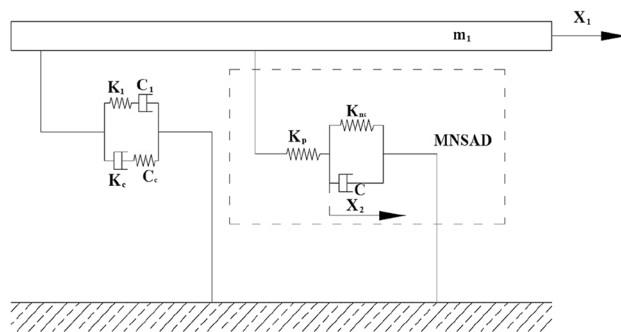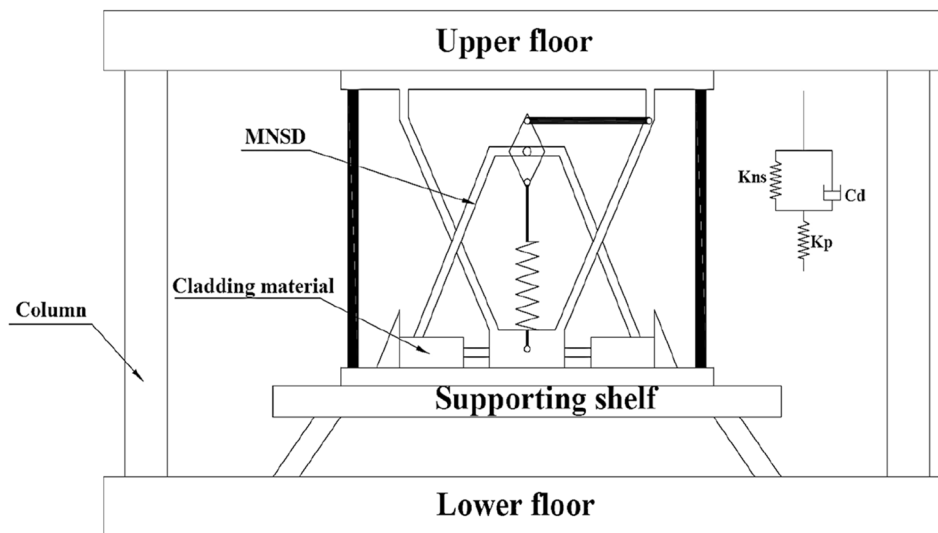

Fig. 3 SDOF systems with a MNSAD of Analytical model

Fig. 2 MSAD Physical Realisation

the MNAD is represented by x_2 of the MNSAD dashpot. Also, derivative with respect to time is represented as dots.

$$w_1 = \sqrt{\frac{k_1}{m_1}}, \ \xi_1 = \frac{c_1}{2w_1m_1}, \ \xi_2 = \frac{c_c}{2w_2m_2}, \ \alpha = \frac{k_{ns}}{k_1} \ and \ \gamma = \frac{k_2}{k_1} \tag{4}$$

We get the following by inserting Eq. (2) into Eq. (1):

$$\begin{cases} \ddot{x}_1 + 2\xi_1 w_1 \dot{x}_1 + w_1^2 x_1 + \gamma w_1^2 (x_1 - x_2) = -\ddot{x}_g - P(t) \\ 2\xi_1 w_1 \dot{x}_2 + \alpha w_1^2 x_2 = \gamma w_1^2 (x_1 - x_2) \end{cases} \tag{5}$$

where ξ_1, γ and α show the damping ratio, stiffness ratio, and negative stiffness ratio of the MNSAD, respectively.

$$H(s) = \frac{(\alpha + \gamma)w_1^2 + 2\xi_2 w_1 s}{\left[(1+\gamma)w_1^2 + s^2 + 2\xi_1 w_1 s\right]\left[(\alpha+\gamma)\gamma w_1^2 + 2\xi_2 w_1 s\right] - \gamma^3 w_1^4} \tag{6}$$

where s = iw stand for the complex frequency and i=$\sqrt{-1}$ is the imaginary part. By substituting $\lambda = {}^w\!/_{w_1}$ in the Eq. (6) we have:

$$H(iw)w_1^2 = \frac{(\alpha + \gamma) + 2\xi_2 \lambda i}{\left[1 + \gamma - \lambda^2 + 2\xi_1 \lambda i\right]\left[(\alpha + \gamma) + 2\xi_2 \lambda i\right] - \gamma^2} = \frac{A + Bi}{C + Di} \tag{7}$$

where

$A = \alpha + \gamma, B = 2\xi_2 \lambda, C = (1 + \gamma - \lambda^2)(\alpha + \gamma) - \gamma^2 - 4\xi_1\xi_2\lambda^2$ and $D = 2(1 + \gamma - \lambda^2)\xi_2\lambda + 2(\alpha + \gamma)\xi_1\lambda$

Finally, the Square transfer function and the amplitude transfer function is derived as below:

$$R(\lambda) = \frac{A^2 + B^2}{C^2 + D^2} \tag{8}$$

$$A(\lambda) = \sqrt{\frac{A^2 + B^2}{C^2 + D^2}} \tag{9}$$

2.3 Damping effect of the MNSAD

This section discusses the effect of MNSAD on the damping ratio of an SDOF system. To this end, three parameters α, γ and ξ_2 are used to assess the performance of the system equipped with MNSAD. The horizontal tangent points with different damping ratios are considered for the analysis of the MNSAD. Figure 4 shows the adjusting values of ξ_2 for the curve of the SDOF system with MNSAD. More details about the performance of the NSAD with different ξ_2 are provided in [66].

Figure 4 shows the amplitudes of the primary SDOF system for different MNSAD dampings (γ=0.5, α=− 0.25). The NSAD system equals two series connected the spring
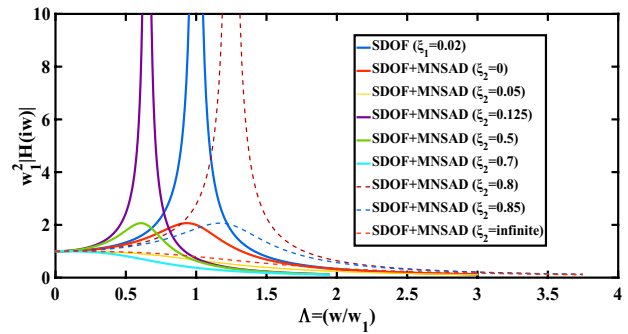
Fig. 4 Primary SDOF system amplitudes for various MNSAD dampings (γ=0.5, α=− 0.25)

for ξ_2=0 (See Fig. 1c). Also, from Eq. (1), we have k_{TE}=− 0.5k_1; thus, for $\lambda > 1$, peak resonant frequency occurs when no energy dissipations occur so that NSAD will be equal to positive stiffness spring k_p. NSAD dashpot will be locked together (i.e., i and s in Fig. 1a) when the damping of the NSAD dashpot reaches a considerable value $\xi_2 = \infty$.

Maximum energy dissipation capacity is observed for the optimal value of the MNSAD. As a result, all of the curves will begin at the same point, indicating that MNSAD has changed its damping coefficient. The detailed optimum procedure is described in the following section.

3 MNSAD optimal design method for SDOF systems

Three criteria are critical in determining the performance of the MNSAD under blast conditions, which are α, γ and ξ_2. The suggested connecting stiffness ratio γ is used to determine the optimal negative stiffness ratio α. The following assumptions are taken into account for determining the appropriate MNSAD settings.

i. Transfer functions attain the same value at two fixed points (i.e., P and Q in Fig. 4) [67].
ii. The highest value of the transfer function in Fig. 4 is at a non-zero fixed point.
iii. For the sake of simplicity, we ignore the SDOF system's intrinsic dampening.

3.1 Transfer function of the fixed point

In the first step, the fixed points P locations are determined by modifying Eq. (8) as follows:

$$R(\lambda) = \frac{(\alpha + \gamma)^2 + (2\xi_2\lambda)^2}{\left[(1 + \gamma - \lambda^2)(\alpha + \gamma) - \gamma^2 - 4\xi_1\xi_2\lambda^2\right]^2} \tag{10}$$
$$+ \left[2(1 + \gamma - \lambda^2)\xi_2\lambda + 2(\alpha + \gamma)\xi_1\lambda\right]^2$$

By substituting $\xi_2 = 0$ and $\xi_2 = \infty$ in the above equation, we have:

$$R_0 = R_{\xi_2=0} = \frac{(\alpha + \gamma)^2}{\left[(1 + \gamma - \lambda^2)(\alpha + \gamma) - \gamma^2\right]^2 + \left[2(\alpha + \gamma)\xi_1\lambda\right]^2} \tag{11}$$

$$R_\infty = R_{\xi_2=\infty} = \frac{(2\gamma)^2}{\left[4\xi_1\lambda^2\right]^2 + \left[2(1 + \gamma - \lambda^2)\lambda\right]^2} \tag{12}$$

By simplifying Eq. (12), the following formula. is obtained:

$$R(0) = \frac{(\alpha + \gamma)^2}{\left[(1 + \gamma)(\alpha + \gamma) - \gamma^2\right]^2} \tag{13}$$

Accordingly, the locations of the fixed point are obtained by:

$$\lambda_p = \sqrt{1 + \gamma - \frac{\gamma^2}{2(\alpha + \gamma)}} \tag{14}$$

3.2 Optimized negative stiffness ratio

MNSAD increases the static response of SDOF systems to minimize system stiffness. Hence, It is not boosting the higher response of zero frequency stimulation for lower response by providing the proper value of α. According to the assumptions, the values of the transfer functions at two points P and Q are the same as:

$$R_0(\lambda_p) = H^2(0) \tag{15}$$

Accodringly, Eq. (15) is reformulated based on the final assumptions, ignoring the inherent damping ξ_1.

$$\frac{(\alpha + \gamma)^2}{\left[(1 + \gamma - \lambda_p^2)(\alpha + \gamma) - \gamma^2\right]^2} = \frac{(\alpha + \gamma)^2}{\left[(1 + \gamma)(\alpha + \gamma) - \gamma^2\right]^2} \tag{16}$$

It is noteworthy that Eq. (15) is transformed since λ_p^2 is a non-zero term, so we have:

$$\left(1 + \gamma - \lambda_p^2\right)(\alpha + \gamma) - \gamma^2 = \gamma^2 - (1 + \gamma)(\alpha + \gamma) \tag{17}$$

Finally, the optimal negative stiffness ratio is calculated by inserting Eq. (14) into Eq. (17) as follows:

$$\alpha_{opt} = \frac{3\gamma^3}{2(\alpha + \gamma)} - \gamma \tag{18}$$

3.3 Damping ratio of the MNSAD

In this section, Eq. (10) is rewritten with the assumption of ignoring the inherent damping ξ_1:

$$R(\lambda) = \frac{(\alpha + \gamma)^2 + (2\xi_2\lambda)^2}{\left[(1 + \gamma - \lambda^2)(\alpha + \gamma) - \gamma^2 - 4\xi_1\xi_2\lambda^2\right]^2} \tag{19}$$
$$+ \left[2(1 + \gamma - \lambda^2)\xi_2\lambda + 2(\alpha + \gamma)\xi_1\lambda\right]^2$$

The transfer function is obtained under non-zero-point assumptions, which is the MNSAD's optimization criterion.

$$\frac{\delta\sqrt{R(\lambda)}}{\delta\lambda}\bigg|_{\lambda=\lambda_p} = 0 \tag{20}$$

To simplify computations, for optimal MNSAD damping, differentiate the square of the transfer function rather than the transfer function itself [68].

$$\frac{\delta\sqrt{R(\lambda)}}{\delta\lambda}\bigg|_{\lambda^2=\lambda_p^2} = 0 \tag{21}$$

By inserting Eq. (19) into Eq. (21), we reach the following formula:

$$u\frac{\delta v}{\delta\lambda^2} - v\frac{\delta u}{\delta\lambda^2} = 0, when\, \lambda^2 = \lambda_p^2 \tag{22}$$

where

$$u(\lambda^2) = (\alpha + \gamma)^2 + (2\xi_2\lambda)^2 \tag{23}$$

$$v(\lambda^2) = \left[(1 + \gamma - \lambda^2)(\alpha + \gamma) - \gamma^2\right]^2 + \left[2(1 + \gamma - \lambda^2)\xi_2\lambda\right]^2 \tag{24}$$

Differentiate functions $u(\lambda^2)$ and $v(\lambda^2)$ with respect to λ^2 gives:

$$\frac{\delta u(\lambda^2)}{\delta\lambda^2} = 4\xi_2^2 \tag{25}$$

$$\frac{\delta v(\lambda^2)}{\delta\lambda^2} = 2\left[\gamma^2 - (1 + \gamma - \lambda^2)(\alpha + \gamma)\right](\alpha + \gamma) \tag{26}$$
$$+ 4(1 + \gamma - \lambda^2)^2\xi_2^2 + 8(1 + \gamma - \lambda^2)^2\xi_2^2\lambda^2$$

Finally, by plugging Eqs. (23)–(26) into Eq. (22), the optimum damping MNSAD is calculated as shown below:

$$\xi_{2opt} = \frac{\alpha + \gamma}{2\lambda_p} = \frac{\alpha + \gamma}{2\sqrt{1 + \gamma - \frac{\gamma^2}{2(\alpha+\gamma)}}} \qquad (27)$$

4 Optimal

4.1 MNSAD with SDOF systems

Figure 5 depicts comparisons of uncontrolled SDOF systems with SDOF systems with cladding, SDOF systems with MNSAD, and SDOF systems with cladding and MNSAD systems taking transfer function into account. It can develop the optimal MNSAD utilizing Eqs. (18)–(27). The parameters of the three systems are shown in Table 1.

Figure 5 demonstrates that by employing cladding material, the resonant frequency ratio of the SDOF system is decreased to 50%, the resonant frequency ratio of the SDOF system and MNSAD is reduced to 75%, and the resonant frequency ratio of the SDOF system, MNSAD, and cladding is reduced to 83%. Also, it shows stiffness and damping ratio comparisons with various SDOF system combinations. A considerable damping effect is accomplished by adding a small amount of damping ($\xi_2 = 2.8\%$) to the SDOF system with MNSAD. The dampening effect of an SDOF system with MNSAD is superior to that of an SDOF system with a cladding system.
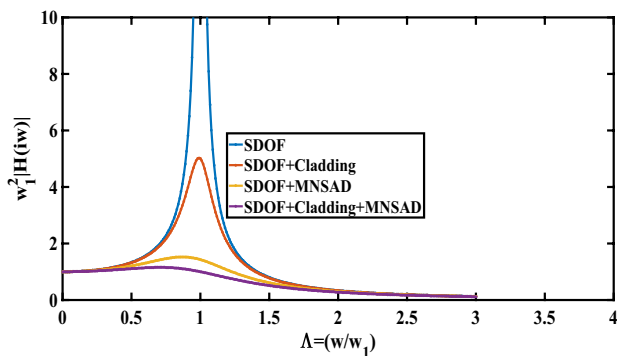
Since total equivalent stiffness is reduced in the negative stiffness damper, providing extra stiffness to the structural system to replace the overall stiffness losses as K Damper does reduce the static response of the original structural system [69–71]. The primary goal of the paper is to preserve the reductions in displacement and accelerations of the SDOF system due to the negative stiffness property of the MNSAD while avoiding the addition of extra compensating stiffness.

5 Proposed algorithm

The proposed algorithm for calculating the response of the SDOF system exposed to air blast load is shown in Fig. 6. The first step is to enter the parameters for the SDOF system's mass matrix, stiffness matrix, and damping matrix. The second step is to perform a non-linear dynamic analysis using Newmark's beta method, followed by calculating the maximum response of the SDOF system. The displacement, velocity, accelerations, pressure, and impulse are all part of the response. The force exerted by the modified negative stiffness amplifying damping, the cladding material, and the MNSAD & Cladding material combinations are calculated. The response of the bare SDOF system controls the force exerted by the control device.

The three parameters of stiffness ratio, damping ratio, and negative stiffness ratio are critical in the operation of the negative stiffness damper. For the force exerted by the MNSAD, the optimal design parameter of negative stiffness is taken into account. The control device with the SDOF system absorbs or dissipates the energy dissipated by the blast load.

6 Stochastic response of SDOF system with MNSAD

This section investigates MNSAD's stochastic response. Comparisons are made between bare SDOF systems and SDOF systems with MNSAD, cladding, and combinations of MNSAD and cladding with SDOF systems.
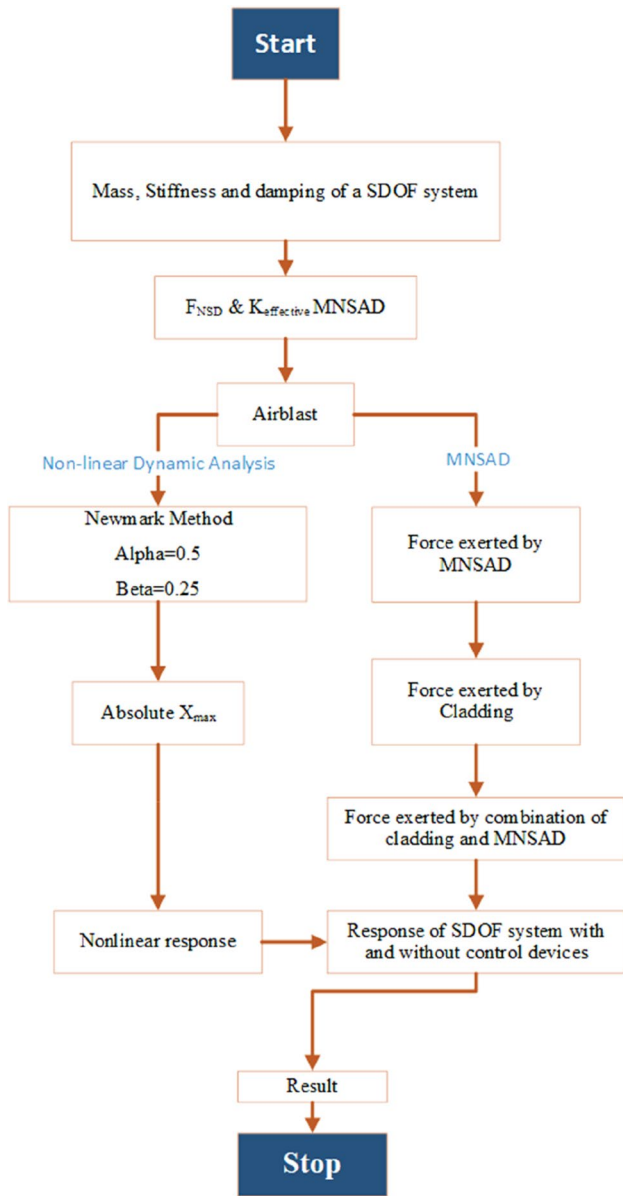

Fig. 5 Comparisons of an uncontrolled SDOF system with a controlled SDOF system with Cladding and MNSAD

Table 1 Uncontrolled SDOF system, SDOF system with cladding material, MNSAD

Parameter	SDOF	SDOF + Cladding	SDOF + MNSAD	SDOF + MNSAD + Cladding
ξ_1	2.5%	1.5%	0.8%	2.85%
γ	0.45	0.25	0.35	0.158
ξ_2	1.45%	20.85%	33.1%	34.5%
α	0.15	–	–	–

Fig. 6 Flowchart of the developed algorithm [72]

6.1 Stochastic excitations description

The following differential equations excite dynamic vibrations and can be approximated as a stationary random process $\ddot{x}_g$. The Clough–Penzien model uses classical dynamic vibrations to simulate excitations [73–75] as shown below:

$$\ddot{x}_g(t) + 2\xi_f w_f \dot{u}_g(t) + w_f^2 u_g(t) = \ddot{u}_f(t) + \ddot{u}_o(t) \tag{28}$$

$$\ddot{u}_f(t) + 2\xi_g w_g \dot{u}_f(t) + w_g^2 u_f(t) = -\dot{u}_o(t) \tag{29}$$

where $\ddot{u}_o(t)$ is the constant intensity of white noise random process, $w_g = 2\pi/T_g$ shows the site of dominant frequency,

(a). 0.5 Sec

(b). 1.0 Sec

(c). 3.0 Sec
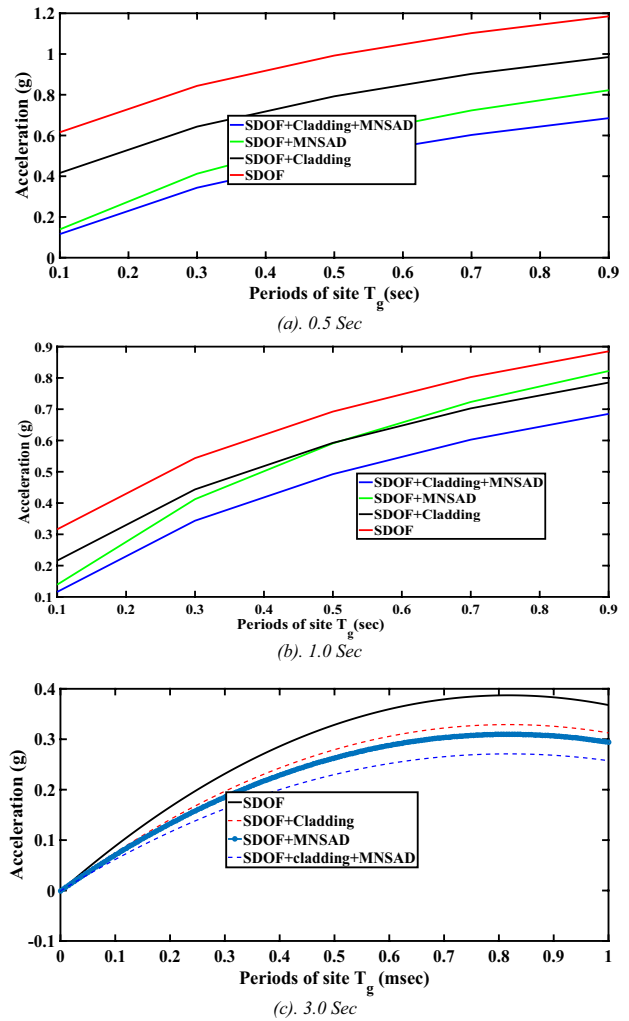
Fig. 7 Absolute acceleration responses for different systems with the influence of site period

ξ_g is the damping ratio of the site, $w_f = 2\pi/T_f$ denotes the location of the dominant frequency and ξ_f is the correction parameters of the Clough Penzien model.

Combining Eqs. (2) and (29) yields the parameters studied of stochastic responses of SDOF systems with MNSAD (29).

6.2 Impact of the site period

Figure 7 depicts the effect of site period on acceleration response. The bold line represents the performance of SDOF and MNSAD combinations, while the black line represents the bare frame of the SDOF system, the red dotted line indicates SDOF and cladding material system combinations, and the blue dotted line indicates SDOF system with cladding material and MNSAD system combinations.
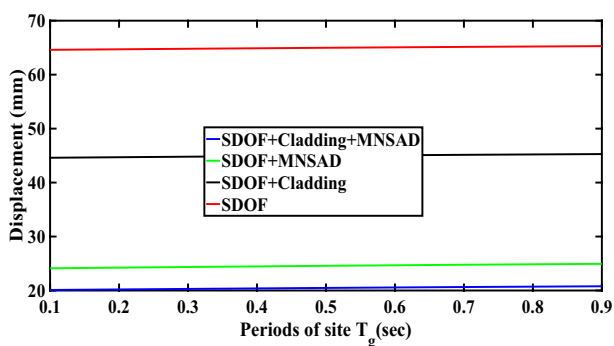
Figure 7a depicts the 0.5 s site period of the SDOF system with and without control devices. The Site period increases
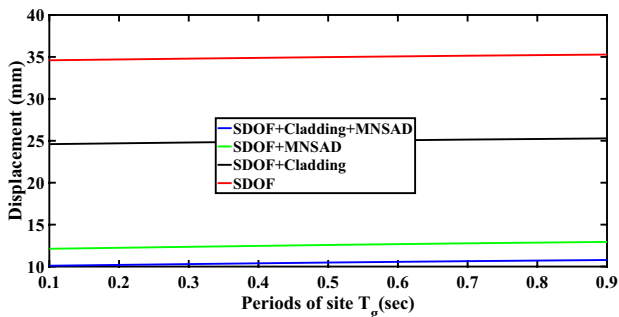
until a certain value is reached and then decreases. The maximum acceleration of the bare SDOF system is 1.2 g, which is reduced to 1 g, 0.82 g, and 0.65 g with the SDOF and cladding, SDOF and MNSAD, and SDOF, Cladding, and MNSAD combinations, respectively. Figure 7b depicts the 1.0 s site period of the SDOF system with and without control devices. The Site period increases until a certain value is reached and then decreases.

The maximum acceleration of the bare SDOF system is 0.88 g, which is reduced to 0.82 g, 0.78 g, and 0.69 g with the SDOF and cladding, SDOF and MNSAD, and SDOF, Cladding, and MNSAD combinations, respectively. Figure 7c depicts the 3.0 s site period of the SDOF system with and without control devices. The acceleration profile

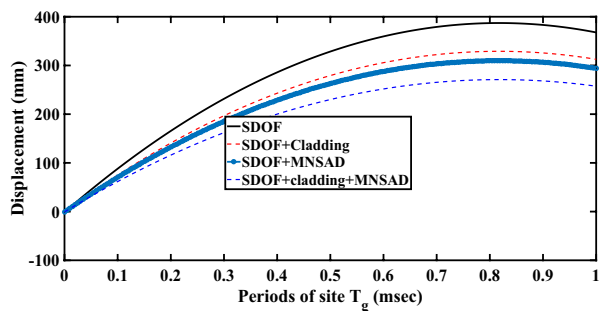is a straight line. With the control device combinations, the accelerations profile dimness.

The displacement response of the uncontrolled SDOF system and combinations of the SDOF system with cladding
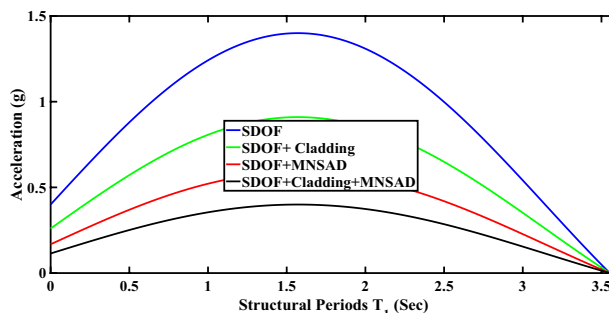
(a) Mean value of displacement
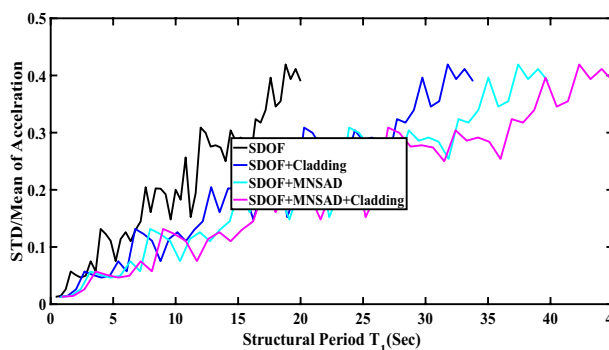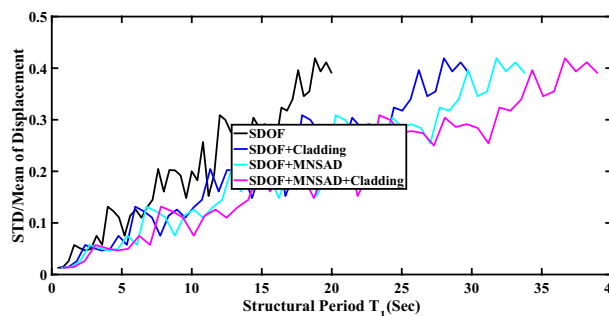
(a). 0.5 Sec

(b) Mean value of acceleration

(b). 1.0 Sec

(c) Coefficient of variance of displacement

(c). 1.5 Sec
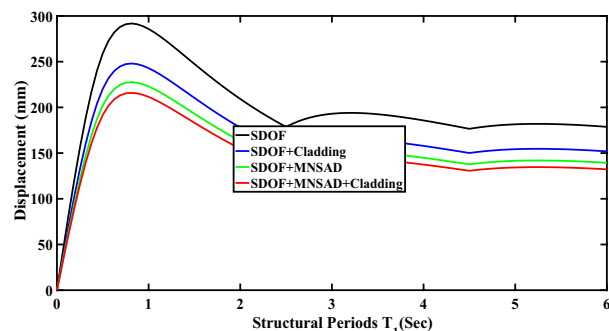
(d) Coefficient of variance of acceleration

Fig. 8 Different systems of the SDOF responses on the displacement of the influence site period

Fig. 9 Control of the SDOF system's response by a control device subjected to air blast load

Table 2 Various systems with maximum responses with the variance of the site period

| Maximum response value	Site period	Statistical parameters	Bare SDOF	SDOF + Cladding	SDOF + MNSAD
Displacement (mm)	$T_1 = 0.5$ S	Mean	321.08	282.3	118.23
		STD	6.80	5.28	4.18
		STD/Mean	0.175	0.0958	0.0785
	$T_1 = 1.0$ S	Mean	9113.28	8953.12	7852.3
		STD	218.32	208.45	194.6
		STD/Mean	0.325	0.285	0.248
	$T_1 = 3.0$ S	Mean	0.7258	0.6852	0.6682
		STD	0.243	0.232	0.218
		STD/Mean	0.168	0.528	0.4825
Acceleration (g)	$T_1 = 0.5$ S	Mean	0.528	0.489	0.398
		STD	0.0853	0.0785	0.0689
		STD/Mean	0.321	0.238	0.221
	$T_1 = 1.0$ S	Mean	0.1406	0.1346	0.1258
		STD	0.0456	0.0385	0.0285
		STD/Mean	0.365	0.315	0.280
	$T_1 = 3.0$ S	Mean	0.0245	0.0185	0.0175
		STD	0.443	0.410	0.320
		STD/Mean	0.285	0.262	0.158
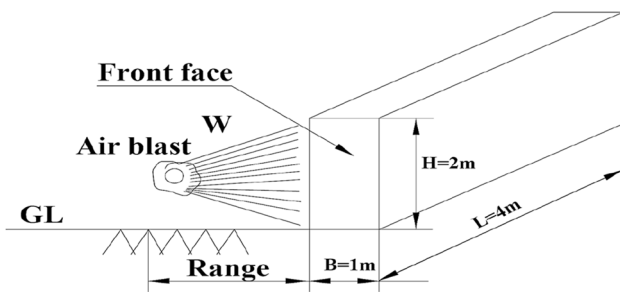
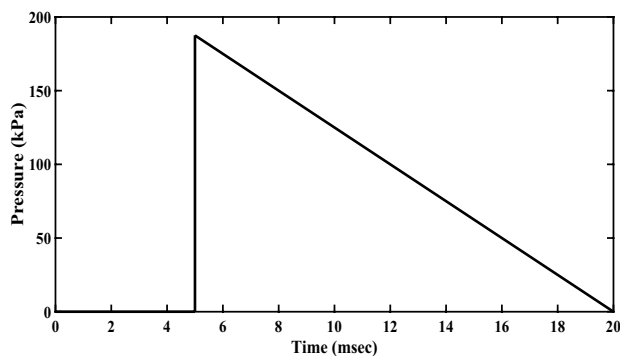**Fig. 10** Typical air blast load occurring in the SDOF system

Fig. 11 Air blast load acting on the SDOF system

considered: 0.5 s, 1.0 s, and 1.5 s. The displacement is reduced by combining the SDOF system's various devices.

The middle long period structure indicates the maximum period of the site (T1 = 1.0 s), as shown in Figs. 7b and 8b, the three systems of the structural response with an increase in site period. At the low damping ratio and low cost of the SDOF system, both displacement and acceleration are reduced by 35% and 42%, respectively. In the long period (T1 = 3.0 s), the period of all three structural systems is greater than the maximum site period, as shown in FigS. 7c and 8c.

6.3 Impact of structural period

Three different systems of the SDOF stochastic response with the impact of the structural period are depicted in Fig. 9. The mean displacement increases and gradually decreases in long period structures. The site period (Tg = 0.5 s) of three structural systems means that acceleration response increases, reaching maximum structural period values and then gradually decreasing. Table 2 shows the detailed percentage of reductions in SDOF response with control devices.

material and MNSAD of the influence of the site period are shown in Fig. 8. The three different site periods are

7 Evaluation of the MNSAD under air blast load

The air blast load is taken into account for the study's analysis among the various blast loads. The air blast occurs in the air medium and the rapid release of energy results in

Table 3 Dynamics properties of Kanai-Tajimi model of SDOF system

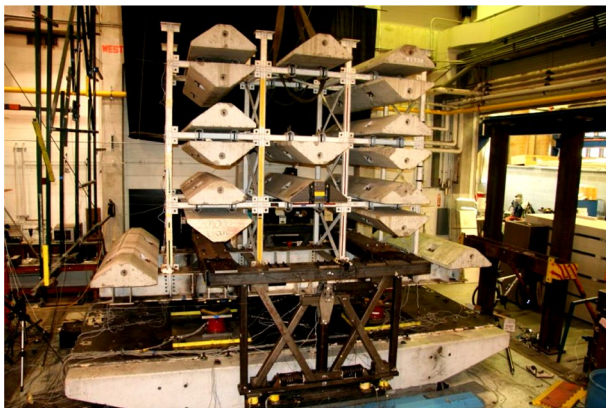| Parameter	Symbol	Default values	Variation of range
Period of SDOF systems	T_1	0.5, 1.0, 3.0 s	0.1–0.4 s
Damping of Inherent of SDOF system	ξ_1	2%	–
Period of the site	T_g	0.5 s	0.5~2 s
Damping of the site	ξ_g	0.6	–
Correction period	T_f	$0.2T_g$	–
Correction damping	ξ_f	ξ_g	–

Fig. 12 Three storey base isolated structure with NSD installations [81]

Fig. 13 Amplitudes of the primary SDOF system with NSAD damping at $\gamma = 0.5$, $\alpha = -0.25$
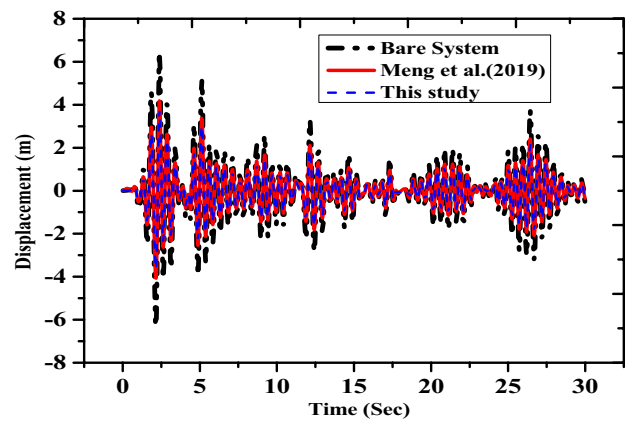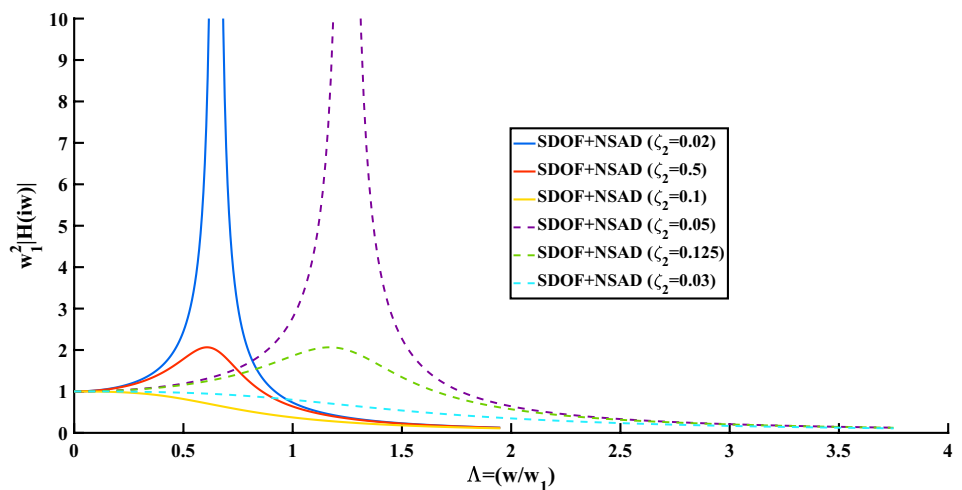

Fig. 14 Comparisons of displacement of SDOF system by Meng et al. (2019) and the current study under a dynamic loading

the occurrence of the blast wave [76, 77]. The explosive air creates the blast wave and travels outward, interacting with everything in its path. The interaction of the wave with the object results in the failure of the structure or the object due to dynamic and impact loads imposed on the object.

The amount of energy released by the explosive in terms of pressure. Under-pressure is smaller in magnitude and lasts longer than positive pressure, after which overpressure occurs. The magnitude of the overpressure influences the explosive, standoff distance, and detonation points [78, 79].

Figure 10 depicts a typical air blast load in the SDOF system. The width, length, and height of the corresponding dimensions of the SDOF system are 1 m, 4 m, and 2 m, respectively. The weight of the air blast load W occurs at a distance known as a range from the SDOF system [80]. The standoff distance is the height of the air blast load distance that occurs above ground level. Blast load occurs in our case on the front face of the SDOF system.
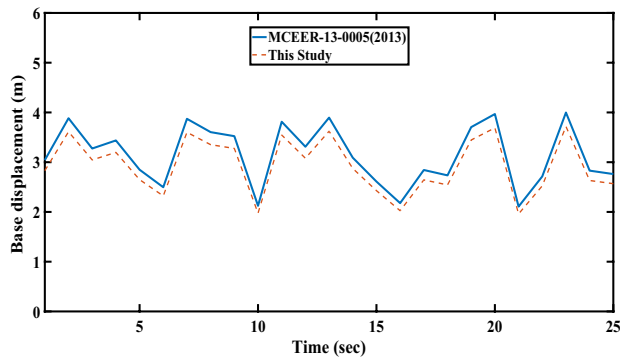
Fig. 15 Comparisons of base displacement of the model with NSD by MCEER-13-0005(2013) and the current study under a dynamic loading

The air blast load is calculated using the equations listed below. The shock density of the jump is determined by Rankine–Huguenot jump conditions [81].

$$\rho_s = \rho_o \frac{(1 + \gamma)P_{so} + 2\gamma P_o}{(\gamma - 1)P_{so} + 2\gamma P_o} \tag{30}$$

$$u_s = P_{so}a_o \sqrt{\frac{2}{\gamma P_o\left[(\gamma + 1)P_{so} + 2\gamma P_o\right]}} \tag{31}$$

where ρ_s is the density of the shock front, ρ_o, P_o and a_o are the density, pressure and sound speed at ambient pressure in air, respectively, u_s shows the shock front velocity, γ depicts the specific heat ratio (for air, it is 1.4). Figure 11 depicts the magnitude of the air blast load in the SDOF system. At 5 s, the maximum air blast load is 185 kPa.

8 Validation of SDOF system with NSD

One major step to any analytical and numerical investigation is to validate the modeling procedure with a reliable recent study. In this research, the verification has been done comparing the developed models with two studies by Meng et al. (2019) and MCEER-13-0005 (2013). The first study by Meng et al. 2019 is an analytical simulation, while the MCEER report is an extensive experimental investigation on NSD devices (Fig. 12). The comparison between the results of the current study and the above references are depicted in Table 3 and Figs. 13, 14, and 15.
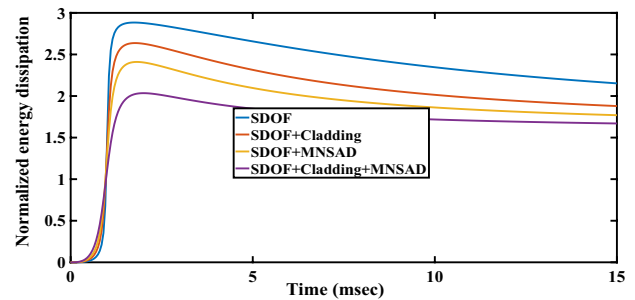
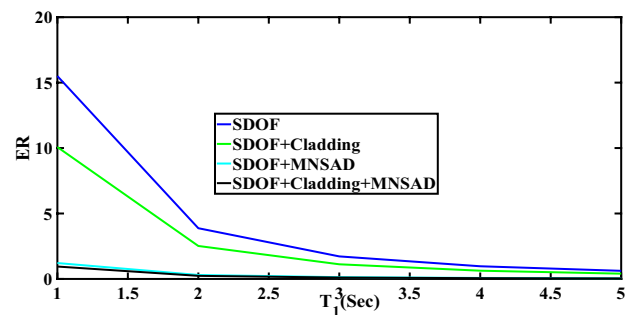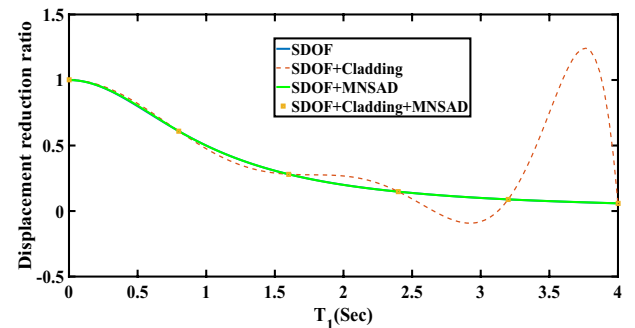*(a). 2% Damping*
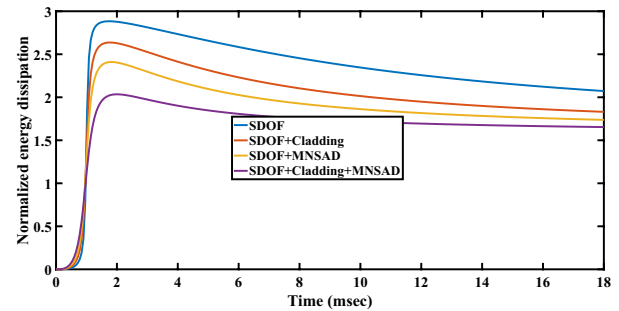
(b). 3% Damping

Fig. 16 Energy dissipated by the SDOF system with various control devices when subjected to an air blast load
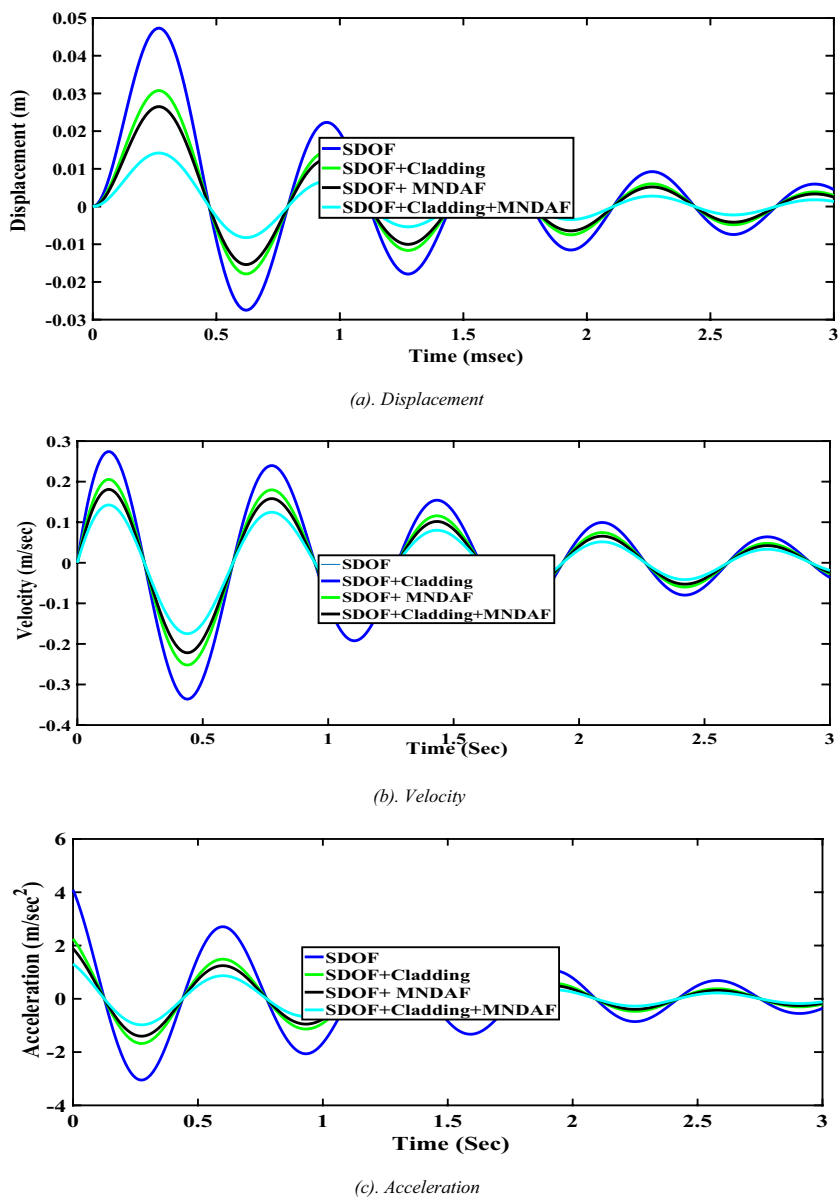

(a). Energy ratio

(b). Displacement ratio

Fig. 17 Energy dissipation ratios of the SDOF system under air blast load

Fig. 18 Control of the SDOF system's response by a control device subjected to air blast load

(a). Displacement

(b). Velocity

(c). Acceleration

Fig. 19 Pressure Impulse curve of SDOF system with different control devices

9 Results and discussions

The response of the SDOF system to an air-blast load is calculated; the response includes displacement, velocity, accelerations, and pressure impulse. In the model studied, the response of the SDOF system is controlled by cladding material and modified negative stiffness amplifying dampers.

9.1 Energy dissipations

Control devices such as cladding material and modified negative stiffness damping are employed to dissipate the energy generated by the air blast load on the SDOF system. Herein, two different damping ratios of 2% and 3% are considered.
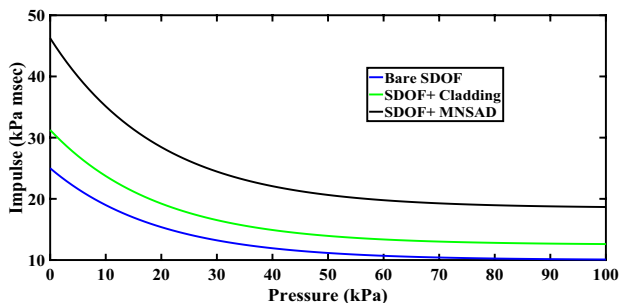
Figure 16a depicts the normalised energy damping dissipations of the SDOF system's 2% damping ratio. Cladding, MNSAD, and combinations of MNSAD and cladding receptively reduce the energy dissipation ratio from 2.8 to 2.6, 2.4, and 2. Figure 15b depicts the normalised energy damping dissipations of the SDOF system's 3% damping ratio. Cladding, MNSAD, and combinations of MNSAD and cladding receptively reduce the energy dissipation ratio from 2.8 to 2.5, 2.34, and 2.1. The energy dissipation ratio increases dramatically at first, then gradually decreases and becomes uniform which is due to the sudden and rapid realisation of energy in a fraction of a second (see Fig. 16).

The energy ratio of the SDOF system with and without control devices is depicted in Fig. 17a. When damping ratios are increased, the energy dissipation capacity of MNSAD does not change significantly when compared to the cladding combinations of the SDOF system. The stiffness ratio is also important for the performance of the SDOF system with MNSAD. The energy ratio of the bare SDOF system is reduced to 10,2 and 1.5 for the cladding, MNSAD, and combining MNSAD and cladding, respectively. The displacement ratio of the SDOF with cladding, SDOF with MNSAD, and SDOF with Cladding and MNSAD system is reduced to 1.3 to 1, 0.8, and 0.6, respectively, as shown in Fig. 17b.

The response reductions of the SDOF system with air blast load are shown in Fig. 18 by using MNSAD and cladding. Figure 19 depicts the progression of the Pressure impulse curve from the bare SDOF system to the SDOF system with cladding and the MNSAD system.

10 Conclusion

The current study focused on the negative stiffness amplifying damper, a novel device proposed with a negative stiffness mechanism and cladding material. The modifying fixed-point methods of the tuned mass damper of the closed-form solution with the closed-form expressions were taken into account. The performance of the MNSAD and the cladding material were stochastically evaluated, investigated, and analytically analyzed in response to the air blast load acting on the SDOF system. Accordingly, the following are the key findings of this study:

   i. When a Cladding material is used, the Negative stiffness spring amplifies with the stroke of the dashpot, increasing the MNSAD energy dissipation capacity.

   ii. Using the optimal MNSAD parameters, the resonant response of the SDOF system is reduced with the same total damping coefficient.

   iii. Changes in the damping ratio do not affect the connecting stiffness ratio, and the MNSAD's negative stiffness ratio is prescribed with the transfer function in mind.

   iv. By conducting the stochastic response analysis of the MNSAD, the maximum response of the displacement and accelerations is reduced by approximately 60%, with a small damping ratio of 2.8% and coefficient variance of more than 30%.

   v. With an energy dissipation capacity of less than 2%, MNSAD improves the energy dissipation capacity by 6–16 times by employing a small damping coefficient.

Declarations

Competing interests/Conflict of interest The author(s) declared no potential conflicts of interest concerning the research, authorship, and/or publication of this article.

Ethics approval and consent to participate Not applicable.

Consent for publication Not applicable.

References

1. Richard Curry (2017) Response of plates subjected to air-blast and buried explosions, PhD Report, UNIVERSITY OF CAPE TOWN
2. Landmine montior report (2016) Online, 2016. http://www.the-monitor.org.
3. Army TimesWebsite (2012) March 2012. http://www.armytimes.com/news/2011/02/usatied-toll-in-afghanistan-reduced-by-37-percent-021711/
4. CRS Report on Operation Enduring Freedom (2001) Inside the Air Force, 12(39), 16–18, Washington Publishers. http://www.jstor.org/stable/24790076
5. United Nations website (2016) January 2016. http://www.un.org/apps/news/story.asp?NewsID=39036
6. Fallon C, McShane GJ (2019) Fluid-structure interactions for the air blast loading of elastomer-coated concrete. Int J Solids Struct 168:138–152
7. Al-Thairy H (2016) A modified single degree of freedom method for the analysis of building steel columns subjected to explosion induced blast load. Int J Impact Eng 94:120–133
8. Astarlioglu S, Krauthammer T, Morency D, Tran TP (2013) Behaviour of reinforced concrete columns under combined effects of axial and blast-induced transverse loads. Eng Struct 55:26–34
9. Zhang F, Wu C, Zhao X-L, Xiang H, Li Z-X, Fang Q (2016) Experimental study of CFDST columns infilled with UHPC under close-range blast loading. Int J Impact Eng 93:184–195
10. Ramallo JC, Johnson EA, Spencer BF (2002) Smart base isolation systems. J Eng Mech 128:1088–1099

11. Liu Y, Yan J, Li Z, Huang F (2019) Improved SDOF and numerical approach to study the dynamic response of reinforced concrete columns subjected to close-in blast loading. Structures 22:341–365

12. ASCE (2011) Blast protection of buildings. ASCE/Structural Engineering Institute (SEI) 59–11

13. U.F. Code(UFC) (2008) Structures to resist the effects of accidental explosions. United States of America Department of Defense, Washington, D.C.

14. Dragos J, Wu C (2014) Single-degree-of-freedom approach to incorporate axial load effects on pressure impulse curves for steel columns. J Eng Mech 141:04014098

15. Wang W, Zhang D, Lu F, Wang S-C, Tang F (2012) Experimental study on scaling the explosion resistance of a one-way square reinforced concrete slab under a close-in blast loading. Int J Impact Eng 49:158–164

16. Kiran KK, Kori JG (2018) Controlling blast loading of the structural system by cladding material. Comput Eng Phys Model 1(3):79–99

17. US DoD (Department of Defence) (2008) Structures to resist the effects of accidental explosions. Washington DC, USA: US DoD; 2008. pp.1e1867.UFC-3–304–02.

18. U.S. Army Corps of Engineers (2008) Me 1 thodology manual for the single-degree-of freedom blast effects design spreadsheets (SBEDS); 2008. pp. 1.1–10.4. PDCTR-06e01

19. Cormie D, Mays G, Smith P (2009) Blast effects on buildings, 2nd edn. Thomas Telford, London, pp 13–56

20. Rigby SE, Tyas A, Bennett T (2014) Elastic-plastic response of plates subjected to cleared blast loads. Int J Impact Eng 66:37–47

21. Rigby SE, Tyas A, Bennett T (2012) Single-Degree-of-Freedom response of finite targets subjected to blast loading—the influence of clearing. Eng Struct 45:396–404

22. Wang W, Zhang D, Fangyun LF, Liu R (2013) A new SDOF method of one-way reinforced concrete slab under non-uniform blast loading. Struct Eng Mech 46(5):595–613

23. Fischer K, Häring I (2009) SDOF response model parameters from dynamic blast loading experiments. Eng Struct 31:1677–1686

24. El-Dakhakhni WW, Mekky WF, Changiz Rezaei SH (2010) Validity of SDOF models for analysing two-way reinforced concrete panels under blast loading. J Perform Constr Facil 24:311–325

25. Newmark NM, Hansen RJ (1961) Design of Blast resistant structures, shock and vibration handbook. Mc Graw-Hill, New York

26. Pannil F, Kingery NC (1964) Peak overpressure vs scaled distance for tnt surface bursts (Hemispherical Charges). Ballistic Research Laboratories, Defense Documentation Center, Alexandria

27. Henrych J, Rudolph M (1979) The dynamics of explosion and its use. Elsevier, Amsterdam

28. Swisdak MM (1994) Simplified Kingery air-blast calculations. Minutes of the Twenty Sixth DoD Explosives Safety Seminar, Maryland

29. Remennikov MA (2003) A review of methods for predicting bomb blast effects on buildings. J Battlef Technol 2(3):5–10

30. Remennikov A, Carolan D (2006) Blast effects and vulnerability of building structures from terrorist attack. Austr J Struct Eng 7(1):1–11. https://doi.org/10.1080/13287982.2006.11464959

31. Shariq M, Haseeb S, Arif M (2017) Analysis of existing masonry heritage building subjected to earthquake loading. In: 11th International Symposium on Plasticity and Impact Mechanics, Implast, Elsevier, Vol. 173, pp 1833–1840

32. Richards BA (2008) Prediction and control of air overpressure from blasting in Hong Kong. geo report no. 232. Hong Kong: Geotechnical Engineering Office, Civil Engineering and Development Department

33. Hao H (2009) Numerical modelling of masonry wall response to blast loads. Aust J Struct Eng 10(1):37–52

34. Wu C, Fattori G, Whittaker A, Oehlers JD (2010) Investigation of air-blast effects from spherical and cylindrical-shaped charges. Int J Prot Struct 1(3):345–362

35. Ahmad S, Elahi A, Pervaiz H, Rahman AG, Barbhuiya S (2014) Experimental study of masonry wall exposed to blast loading. Mater de Constr 64(313):1–11

36. Anas SM, Ansar MI, M Alam M (2020) Performance of masonry heritage building under air-blast pressure without and with ground shock. Austr J Struct Eng 21(4):329–344

37. Chen C, Wang X, Hou H, Cheng Y, Zhang P, Liu J (2020) Effect of strength matching on failure characteristics of polyurea coated thin metal plates under localised air blast loading: experiment and numerical analysis. Thin-Walled Struct 154:106819

38. Xu S, Wen H, Liu B, Guedes Soares C (2020) Experimental and numerical analysis of dynamic failure of welded aluminium alloy plates under air blast loading. Ships Offshore Struct 17(3):531–540. https://doi.org/10.1080/17445302.2020.1835076

39. Li S, B Yu B, Karagiozova D, Liu Z, Lu G, Wang Z (2019) Experimental, numerical, and theoretical studies of the response of short cylindrical stainless-steel tubes under lateral air blast loading. Int JImpact Eng 124:48–60

40. Redekop D, Azar P (1991) Dynamic response of a cylindrical shell panel to explosive loading. J Vib Acoust Stress Reliab 113(3):273–278

41. Li Q, Jones N (1995) Blast loading of a short cylindrical shell with transverse shear effects. Int J Impact Eng 16(2):331–353

42. Molyneaux WG (1957) Supports of vibration isolation. ARC/CP-322, Aeronautical Research council, U.K.

43. Nagarajaiah S, Reinhorn AM, Constantinou MC, Taylor D, Pasala DTR, Sarlis AA (2010) Adaptive negative stiffness: a new structural modification approach for seismic protection. In: Proc., 5th World Conf. on Structural Control and Monitoring. Tokyo: International Association for Structural Control and Monitoring, Univ. of Tokyo

44. Sarlis AA, Pasala DTR, Constantinou MC, Reinhorn AM, Nagarajaiah S, Taylor DP (2013) Negative stiffness device for seismic protection of structures. J Struct Eng 139(7):1124–1133

45. Li HN, Qu C, Huo LS, Nagarajaiah S (2016) Equivalent bilinear elastic single degree of freedom system of multi-degree of freedom structure with negative stiffness. J Sound Vib 365:1–14

46. Iemura H, Pradono MH (2009) Advances in the development of pseudo-negative-stiffness dampers for seismic response control. Structural Control Health Monit 16:784–799

47. Dijkstra K, Videc BP, Huizinga J (1988) Mechanical spring having negative spring stiffness useful in an electroacoustic transducer. J Acoust Soc Am 84:804–810

48. Mizuno T (2003) Vibration isolation system using negative stiffness. JSME Int J Ser C Mech Syst Mach Elements Manuf 46(3):807–812

49. Platus DL (1992) Negative-stiffness-mechanism vibration isolation systems. Vibration Control in Microelectronics. Optics, and Metrology 1619(1):44–54

50. Iemura H, Pradono MH (2002) Passive and semi-active seismic response control of a cable stayed bridge. J Struct Control 9:189–204

51. Li H, Liu J, Ou J (2011) Seismic response control of a cable-stayed bridge using negative stiffness dampers. Struct Control Health Monit 18:265–288

52. Li H, Liu M, Ou J (2008) Negative stiffness characteristics of active and semi-active control systems for stay cables. Struct Control Health Monit 15:120–142

53. Iemura H, Pradono MH (2005) Simple algorithm for semi-active seismic response control of cable-stayed bridges. Earthq Eng Struct Dyn 34:409–423

54. Høgsberg J (2011) The role of negative stiffness in semi-active control of magneto-rheological dampers. Struct Control Health Monit 18:289–304

55. Weber F, Boston C (2011) Clipped viscous damping with negative stiffness for semi-active cable damping. Smart Mater Struct 20:45007

56. Wu B, Shi P, Ou J (2013) Seismic performance of structures incorporating magnetorheological dampers with pseudo-negative stiffness. Struct Control Health Monit 20:405–421

57. Gong W, Xiong S (2016) Probabilistic seismic risk assessment of modified pseudo-negative stiffness control of a base- isolated building. Struct Infrastruct Eng 12:1295–1309

58. Gong W, Xiong S (2017) A new filter-based pseudo-negative-stiffness control for baseisolated buildings. Struct Control Health Monit 24:1912

59. Attary N, Symans MD, Nagarajaiah S, Reinhorn AM, Constantinou MC, Taylor D, ... Sarlis AA (2012) Performance evaluation of a seismically-isolated bridge structure with adaptive passive negative stiffness. In: Proc. of Fifteenth World Conference on Earthquake Engineering (15WCEE), Tokyo, Japan

60. Sarlis AA, Pasala DTR, Constantinou MC et al (2013) Negative stiffness device for seismic protection of structures. J Struct Eng 139:1124–1133

61. Pasala DTR, Sarlis AA, Nagarajaiah S et al (2013) Adaptive negative stiffness: new structural modification approach for seismic protection. J Struct Eng 139:1112–1123

62. Antoniadis IA, Kanarachos SA, Gryllias K, Sapountzakis IE (2016) K Damping: a stiffness-based vibration absorption concept. J Vib Control 24:193–203

63. Pasala DTR, Sarlis AA, Nagarajaiah S et al (2013) Adaptive negative stiffness: new structural modification approach for seismic protection. J Struct Eng 139:1124–1133

64. Rebelo HB, Cismasiu C (2021) Robustness assessment of a deterministically designed sacrificial cladding for structural protection. Eng Struct 240:112279

65. Khalifa YA, Campidelli M, Tait MJ, El-Dakhakhni WW (2020) Mitigating risk of confined explosion via lightweight sacrificial cladding. J Perform Constr Facil 34(1):04019080

66. Den Hartog J (1995) Mechanical vibrations, 4th edn. Courier Corporation, New York

67. Shen Y, Peng H, Li X, Yang S (2017) Analytical optimal parameters of dynamic vibration absorber with negative stiffness. Mech Syst Signal Process 85:193–203

68. Ikago K, Saito K, Inoue N (2012) Seismic control of single degree of freedom structure using tuned viscous mass damper. Earthq Eng Struct Dyn 41:463–474

69. Antoniadias IA, Kanarachos SA, Gryllias K, Sapountzakis IE (2016) KDamping: a stiffness based vibration absorption concept. SAGE Publications, New York, USA

70. Sapountzaksi EJ, Syrimi PG, Pantazis IA, Antoniadias IA (2017) KDamper concept in seismic isolation of bridges with flexiable piers. Eng Struct 153:525–539

71. Qu C, Li HN, Huo L, Yi TH (2017) Optimum value of negative stiffness and additional damping in civil structures. J Earthq Eng 143:4017068

72. Matlab optimisation toolbox (2012) The MathWorks, Natick, MA, USA

73. Clough RW, Penzien J (1993) Dynamics of structures, 2nd edn. Mc-Graw Hill, New York

74. Giarallis A, Spanos PD (2012) Derivation of response spectrum compatible non stationary stochastic process relying on Monte Carla-based peak factor estimation. Earthq Struct 3(3–4):581–609

75. Biggs JM (1964) Introduction to structural dynamics, 2nd edn. Mc-Graw Hill, New York

76. Kinney GF, Graham KJ (1985) Explosive shocks in air, 2nd edn. The Macmillan Company, New York

77. US Army Corps of Engineers (2008) Structure to resist the effects of accidental explosions. Tech report UFC 3-340-02 formally TM 5-1300, Naval Facilities Engineering Command, Air Force Civil Engineer Support Agency

78. Ben-Dor G, Igra O, Elperin T (2001) Handbook of Shock Waves, volume 1. In: Theoretical, experimental, and numerical technique. Academic Press

79. Hetherington J, Smith P (1994) Blast and ballistic loading of structures. CRC Press, Berlin

80. Wang M, Sun FF, Yang JQ, Nagarajaiah S (2019) Seismic protection of SDOF systems with a negative stiffness amplifying damper. Eng Struct 190:128–141

81. Technical report MCEER-13-0005 (2013) Negative Stiffness devices for seismic protection of the structure June 12, 2013